Least-squares reverse time migration with velocity errors

Jizhong Yang[1], Yunyue Elita Li[1], Arthur Cheng[1], Yuzhu Liu[2], and Liangguo Dong[2]
[1] National University of Singapore, Department of Civil and Environmental Engineering, Singapore 119077.
[2] Tongji University, State Key Laboratory of Marine Geology, Shanghai 200092, China

Summary

An accurate migration velocity model is required for reverse time migration (RTM) to correctly predict the kinematics of wave propagation in the subsurface. Least-squares reverse time migration (LSRTM), which aims to match the amplitudes of the modeled data with the observed data in an iterative inverse procedure, is more sensitive to the accuracy of the migration velocity model. If the migration velocity model contains errors, the final migration images will be defocused and incoherent. As a partial solution, we utilize an LSRTM scheme based on the extended imaging condition, which is called as least-squares extended RTM (LSERTM). It is well accepted that LSERTM can fit the observed data regardless of the accuracy of the migration velocity model. We further explore this property and find that after stacking the extended migration images along the subsurface offset axis within properly selected ranges, we can obtain an image with better coherency and focusing than the conventional LSRTM. We demonstrate the efficacy of our method with numerical examples on a Salt-like model and the Marmousi model.

Introduction

LSRTM aims to seek the approximate inverse rather than the adjoint of the forward modeling operator by iteratively fitting the modeled data with the observed data in a least-squares inverse problem framework. It has the potential to compensate effects caused by the incompleteness of the seismic data due to limited acquisition aperture, coarse source-receiver sampling, band limitation of the source wavelet, and uneven subsurface illumination, and has attracted more and more research interests in recent years (Dai et al., 2012; Zhang et al., 2015; Yang et al., 2016). It has been shown that LSRTM can provide images with higher spatial resolution, more balanced amplitudes, and less migration artifacts than RTM.

The basic assumption for conventional LSRTM is that an accurate migration velocity model is available to correctly predict the traveltime of the observed data, such that only the amplitude differences between the observed and modeled data are matched through the iterative inversion. If errors exist in the migration velocity models, traveltime differences will be introduced and may lead LSRTM to suffer from severe convergence problem, where the final migration images are defocused and incoherent. Luo and Hale (2014) developed an amplitude misfit function for LSRTM that measures amplitude differences after correcting for nonzero traveltime shifts between predicted and observed data using dynamic image warping (DIW). However, accurate prediction of the traveltime shifts using DIW is influenced by the amplitude information, and dependent on the complexity of the velocity model and the acquisition geometry.

Another option is to implement the LSRTM in the shot-record extension domain, in which the migration image of each shot gather is updated separately before the final stacking. Accordingly, this procedure can also be called the prestack LSRTM. Dai and Schuster (2013) first explored this idea in the plane-wave domain. Huang et al. (2016) proposed to accelerate the convergence by using optimal pseudodifferential scaling together with the flexibly preconditioned conjugate gradient algorithm. Liu et al. (2017) implemented the prestack LSRTM with a correlative misfit function. However, the prestack LSRTM are only accurate for mild lateral heterogeneity (Huang et al., 2016). Dai and Schuster (2013), and Liu et al. (2017) admitted that the prestack LSRTM was robust when the migration velocity has bulk errors up to 5%.

In this study, we revisit the concept of LSRTM based on the subsurface offset extended imaging condition, abbreviated as LSERTM (Liu et al., 2013; Hou and Symes, 2016). LSERTM has the capacity to match the observed data no matter the migration velocity model is accurate or not. The curvature of the subsurface offset common image gathers (CIGs) preserves the full kinematic information, together with the migration velocity model. Based on the extended images and the subsurface offsets information, one can further improve the accuracy of the migration velocity model through differential semblance optimization-based migration velocity analysis (Shen et al., 2008; Weibull and Arntsen, 2013; Li et al., 2014). In this paper, we will demonstrate that when the migration velocity model is inaccurate, one can still obtain a subsurface image with better coherency than conventional LSRTM after optimally stacking the migration image along the subsurface offset axis using LSERTM.

The rest of this paper is organized as follows. In the methodology section, we give a brief review of the theory involved with LSRTM and LSERTM. Then, we demonstrate the robustness of LSERTM in the presence of migration velocity errors in the numerical example section. Finally, we give a short summary in the conclusion section.

LSRTM with velocity errors

Methodology

The seismic scattered data in the constant-density acoustic wave equation can be expressed as:

$$d(\boldsymbol{x}_r,\boldsymbol{x}_s,\omega)=\omega^2\sum_{\boldsymbol{x}} f_s(\omega)\boldsymbol{G}_0(\boldsymbol{x},\boldsymbol{x}_s,\omega)\boldsymbol{G}_0(\boldsymbol{x}_r,\boldsymbol{x},\omega)\boldsymbol{m}(\boldsymbol{x}), \quad (1)$$

where ω is the angular frequency, $f_s(\omega)$ is the source signature, $\boldsymbol{m}(\boldsymbol{x})$ denotes the reflectivity (a perturbation to the background velocity model) at imaging point $\boldsymbol{x}$ in the subsurface. $\boldsymbol{G}_0(\boldsymbol{x},\boldsymbol{x}_s,\omega)$ and $\boldsymbol{G}_0(\boldsymbol{x}_r,\boldsymbol{x},\omega)$ are the monochromatic Green's functions from the source $\boldsymbol{x}_s$ to imaging point $\boldsymbol{x}$ and from imaging point $\boldsymbol{x}$ to the receiver $\boldsymbol{x}_r$ in the background medium, respectively.

A standard migrated image $\boldsymbol{m}_{mig}$ can be calculated by applying the adjoint of the forward Born modeling operator to the recorded data (Claerbout, 1992):

$$\boldsymbol{m}_{mig}(\boldsymbol{x})=\sum_{s,r,\omega}\omega^2\left[f_s(\omega)\boldsymbol{G}_0(\boldsymbol{x},\boldsymbol{x}_s,\omega)\boldsymbol{G}_0(\boldsymbol{x}_r,\boldsymbol{x},\omega)\right]^T d(\boldsymbol{x}_r,\boldsymbol{x}_s,\omega). \quad (2)$$

In a matrix notation, the forward Born modeling in equation (1) and the migration in equation (2) can be expressed as:

$$\boldsymbol{d}=\boldsymbol{L}_0\boldsymbol{m}, \quad (3)$$

$$\boldsymbol{m}_{mig}=\boldsymbol{L}_0^T\boldsymbol{d}, \quad (4)$$

where $\boldsymbol{L}_0$ denotes the linearized forward Born modelling operator.

LSRTM aims to solve the reflectivity model $\boldsymbol{m}$ by minimizing the difference between the forward modeled data $\boldsymbol{L}_0\boldsymbol{m}$ and the recorded data $\boldsymbol{d}$ in a least-squares sense:

$$f(\boldsymbol{m})=\frac{1}{2}\left\|\boldsymbol{L}_0\boldsymbol{m}-\boldsymbol{d}\right\|_2^2. \quad (5)$$

However, the success of LSRTM highly relies on the availability of an accurate migration velocity model. Otherwise, the migration image will be defocused and incoherent.

According to the survey-sinking imaging condition introduced by Claerbout (1985), we can introduce an extra subsurface offset to the migration image, when the migration velocity model is inaccurate. Correspondingly, the extended migration image can be computed as:

$$\boldsymbol{m}_{mig}(\boldsymbol{x},\boldsymbol{h})=\sum_{s,r,\omega}\omega^2\left[f_s(\omega)\boldsymbol{G}_0(\boldsymbol{x}-\boldsymbol{h},\boldsymbol{x}_s,\omega)\boldsymbol{G}_0(\boldsymbol{x}_r,\boldsymbol{x}+\boldsymbol{h},\omega)\right]^T d(\boldsymbol{x}_r,\boldsymbol{x}_s,\omega). \quad (6)$$

The seismic scattered data via extended Born modeling can be formulated as:

$$d(\boldsymbol{x}_r,\boldsymbol{x}_s,\omega)=\omega^2\sum_{\boldsymbol{h}}\sum_{\boldsymbol{x}} f_s(\omega)\boldsymbol{G}_0(\boldsymbol{x}-\boldsymbol{h},\boldsymbol{x}_s,\omega)\boldsymbol{G}_0(\boldsymbol{x}_r,\boldsymbol{x}+\boldsymbol{h},\omega)\boldsymbol{m}(\boldsymbol{x},\boldsymbol{h}). \quad (7)$$

Equation (6) and (7) form an adjoint pair of extended migration and forward Born modeling. Similarly, the objective function for LSERTM can be expressed as:

$$f(\boldsymbol{m}(\boldsymbol{x},\boldsymbol{h}))=\frac{1}{2}\left\|\boldsymbol{L}_0(\boldsymbol{x},\boldsymbol{h})\boldsymbol{m}(\boldsymbol{x},\boldsymbol{h})-\boldsymbol{d}\right\|_2^2. \quad (8)$$

Introducing an extra degree of freedom by extending the physical model enables the equalization of model and data dimension, and provides the possibility that we can fit the data regardless of the accuracy of the migration velocity model.

The outputs of LSERTM are non-physical subsurface offset dependent image volumes. Hou and Symes (2015) have shown that, when the migration velocity model is accurate, stacking the extended image volumes over subsurface offsets produces a physical image. However, when the migration velocity model is inaccurate, larger ranges of offset extension should be involved in LSERTM for the aim of fitting the observed data properly. The energy in the subsurface offset CIGs will spread significantly to non-zero offsets. Under such circumstances, stacking over full ranges of subsurface offsets will provide contaminated images. In the next section, we will demonstrate that by properly selecting the offset ranges for final stacking, accurate images could be generated.

Examples

We first apply the LSERTM to a salt-like model shown in Figure 1a. The model dimensions are of 401×151, with 10 m grid intervals. There are 79 shots evenly spaced at 50 m shot intervals, and each shot is recorded with 401 receivers evenly distributed at 10 m receiver spacing. The sources and receivers are on the surface, with the first source and receiver located at distances of 50 and 0 m, respectively. The source time function is a Ricker wavelet with a peak frequency of 30 Hz. The recording time is 2.5 s, with a time interval of 0.5 ms.

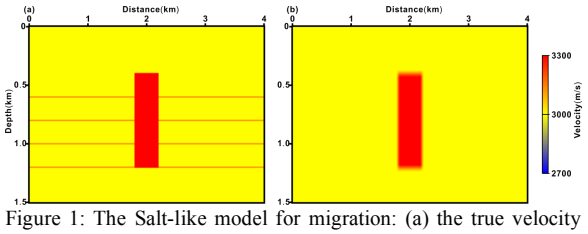

Figure 1: The Salt-like model for migration: (a) the true velocity model, and (b) the accurate migration velocity model.

For reference, we use an accurate migration velocity model as shown in Figure 1b to implement RTM and LSRTM. The corresponding migration images are shown in Figure 2a and 2b, respectively. It is evident that the LSRTM provides better imaging results than RTM with balanced amplitudes and enhanced spatial resolution. However, when an inaccurate homogeneous migration velocity model (v=2700 m/s) is used, the corresponding LSRTM image

becomes defocused and incoherent, which is illustrated by Figure 3a.

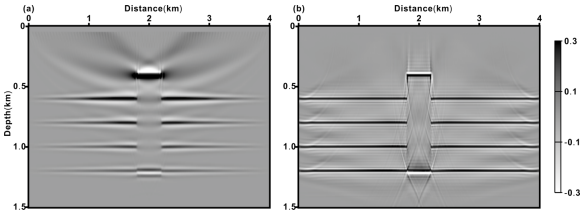

Figure 2: The migration images from (a) RTM, and (b) LSRTM with the accurate migration velocity model.

Then, we implement LSERTM with the same inaccurate migration velocity model. The subsurface offset range is [-300m, 300m], with the offset interval of 10 m. The final image of LSERTM after stacking the extended migration images along the subsurface offset axis [-200m, 200m] is shown in Figure 3b. The LSERTM image after stacking shows clearly better coherence than that of the LSRTM.

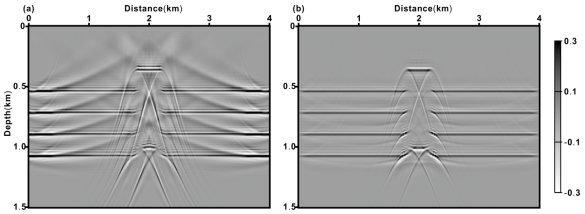

Figure 3: The migration images with the inaccurate homogeneous migration velocity model (v=2700 m/s) from (a) the LSRTM, and (b) the LSERTM after stacking along the subsurface offset axis.

The subsurface offset CIGs (Figure 4a) extracted at the location of x=3000 m are not focused at h=0, which indicates the inaccuracy of the migration velocity model. The data misfit as a function of iteration number is plotted in Figure 4b. It is evident that LSRTM has a good convergence only when the migration velocity is accurate. The LSERTM, on the other hand, shows better convergence than LSRTM in case of an inaccurate migration velocity is used. Figure 5 compares the data residual of LSRTM and LSERTM, respectively. Obviously, LSERTM matches the observed data very well, even though the migration velocity model contains 10% errors for the background, 14% errors for the flat reflectors, and up to 18% errors for the bottom of the salt, respectively. To the contrary, LSRTM fails to reduce the data residual.

From these observations, we conclude that LSERTM is more robust than LSRTM in the presence of velocity errors. However, we should note that although stacking the extended images enhances the image resolution, it does not correct for the mispositioning caused by the velocity error. Another problem is that the vertical salt flanks are not well resolved. This is because the current implementation is mainly focused on utilizing primary reflections, which cannot sufficiently illuminate the steeply dipping structures. To address this issue, we need to further incorporate the prismatic waves in the inversion process, as done in Yang et al. (2017).

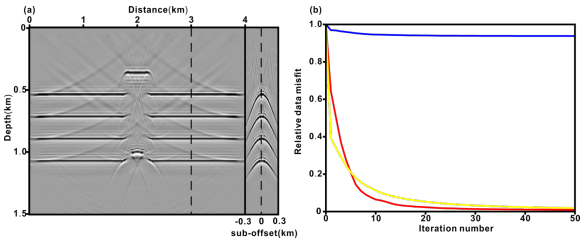

Figure 4: (a) The subsurface offset CIGs from the LSERTM with the inaccurate homogeneous migration velocity model (v=2700 m/s), (b) the relative data misfit plotted as functions of iteration number. The red line denotes the LSRTM with accurate migration velocity model, the blue and yellow lines indicates the LSRTM and the LSERTM with inaccurate migration velocity model, respectively.

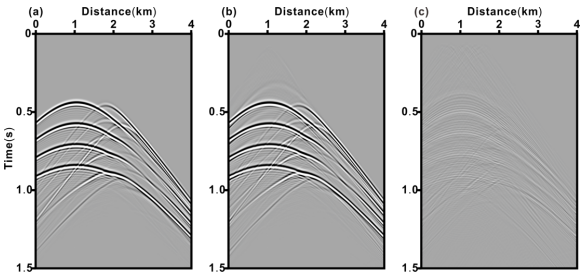

Figure 5: The seismogram of (a) the observed data, (b) the data residual after LSRTM, and (c) the data residual after LSERTM.

We further demonstrate our method with the Marmousi model (Figure 6a). The model dimensions are of 461×170, with 10 m grid intervals. There are 89 shots evenly spaced at 50 m shot intervals, and each shot is recorded with 461 receivers evenly distributed at 10 m receiver spacing. The sources and receivers are on the surface, with the first source and receiver located at distances of 50 and 0 m, respectively. The source time function is a Ricker wavelet with a peak frequency of 20 Hz. The recording time is 3.0 s, with a time interval of 0.5 ms. The migration velocity model, as shown in Figure 6b, is built by smoothing the true velocity model with a 2D Gaussian function whose vertical and horizontal correlation lengths are 400 m, and scaled by a factor of 0.9. The subsurface offset range for LSERTM is [-400m, 400m], with the offset interval of 10 m. Figure 7a and 7b show the images from the LSRTM and the LSERTM after stacking over subsurface offset range [-50m, 50m], respectively. It is apparent that LSERTM image after stacking shows better continuity than LSRTM image, from which we can clearly identify the fault zones and the deep structures inside the anticline.

Conclusions

LSRTM can provide migration images with better quality compared to the standard RTM, only when an accurate migration velocity is available. Inaccurate velocity model can lead to defocused and incoherent images with poor convergence rate. To improve the robustness of the LSRTM in the presence of velocity errors, we have proposed to introduce the extended imaging condition to LSRTM. Numerical examples on a Salt-like model and the Marmousi model provide evidences that: (1) the LSERTM could match the observed data well, even when the migration velocity is inaccurate; (2) by introducing the extended model concept, we have the freedom to handle velocity errors; (3) a physical subsurface image with better continuity than the conventional LSRTM could be obtained after stacking the extended migration images along the subsurface offset axis within properly selected ranges. One thing to note is that, due to the existence of the velocity errors, we are unable to predict the correct positions of the subsurface structures. A potential solution to this problem, which would be a future research topic, is to combine LSERTM with full waveform inversion in a nested way to update the velocity model.

Acknowledgments

The authors would like to thank for the financial supports from the EDB Petroleum Engineering Professorship, the National Natural Science Foundation of China (Grant numbers: 41474034, 41774122, 41674115, and 41630964), the Strategic Priority Research Program of the Chinese Academy of Sciences (Grant No. XDA14010203), and the Open Project (Grant number: MGK1808) of the State Key Laboratory of Marine Geology, Tongji University. Yunyue Elita Li and Jizhong Yang also acknowledge the funding of MOE Tier-1 Grant (Grant numbers: R-302-000-165-133 and R-302-000-182-114).

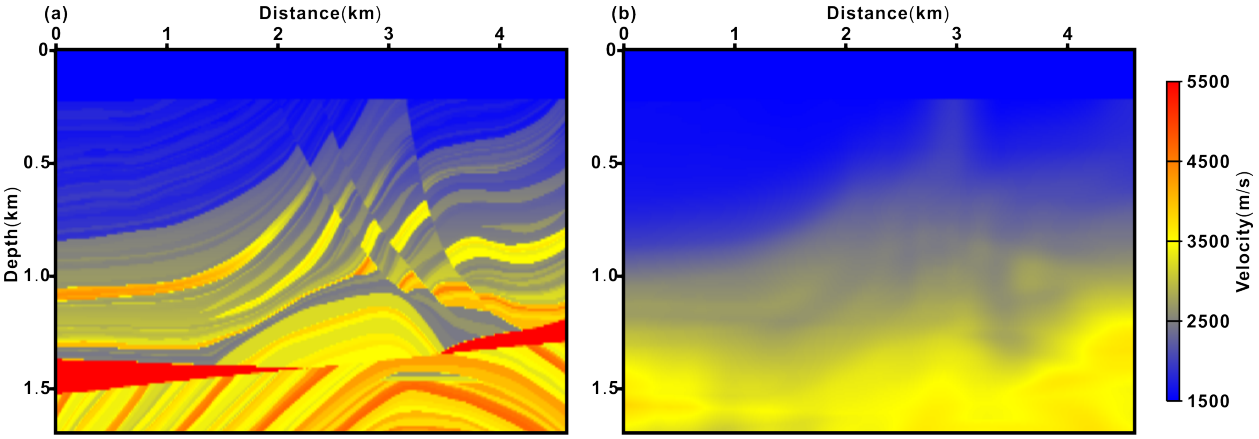

Figure 6: The Marmousi model for migration: (a) true velocity model, (b) migration velocity model.

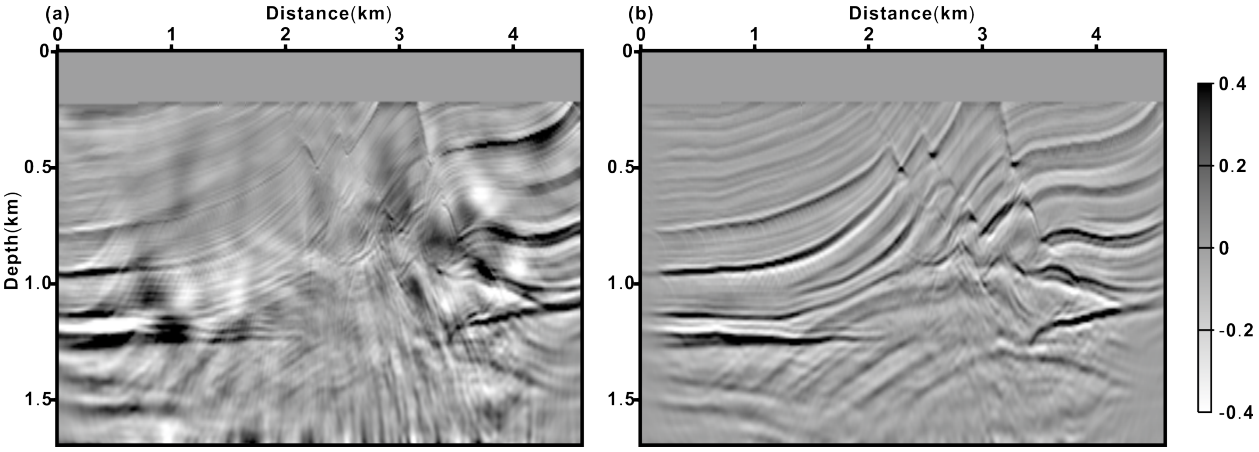

Figure 7: The migration images from (a) the LSRTM, and (b) the LSERTM after stacking along the subsurface offset axis.